Decomposition of $Y_2Ti_2O_7$ Particles in 8 Pct Cr Oxide-Dispersion-Strengthened Martensitic Steel during Tempering

M. TAMURA, H. SAKASEGAWA, K. SHIBA, H. TANIGAWA, K. SHINOZUKA, and H. ESAKA

Chemical composition analysis using inductively coupled plasma spectroscopy and phase identification using X-ray were performed on the extracted residues of 8 pct Cr martensitic steel strengthened by nanoscaled complex oxides, which consist of yttrium, titanium, and oxygen. Some $Y_2Ti_2O_7$ particles, which were stable during normalizing, decomposed into Y_2O_3 and Ti_2O_3 during tempering. This reaction reversibly occurred between normalizing and tempering. $Y_2Ti_2O_7$ particles formed in the steel had other constituents in solid solution as compared to the completely stoichiometric $Y_2Ti_2O_7$ particles synthesized artificially in air. As for the mechanism of the decomposition of $Y_2Ti_2O_7$ particles in the steel, segregation of oxygen to dislocations induced by normalizing caused the decomposition of $Y_2Ti_2O_7$ during tempering. In addition to that, the interfacial strain between Y_2O_3 particles or Ti_2O_3 particles within $Cr_{23}C_6$ carbides, which are formed by tempering, was lower than the strain between $Y_2Ti_2O_7$, which precipitated in $Cr_{23}C_6$ carbides or the matrix. This difference in interfacial strain could also promote the decomposition of the $Y_2Ti_2O_7$ particles in the steel.

I. INTRODUCTION

THE experimental fusion reactor, ITER, is under construction in France, and the first plasma should possibly ignite by 2026. Structural materials of the Japanese test blanket module for ITER have been designed using a reduced activation ferritic/martensitic (RAFM) steel, F-82H.[1,2] However, the maximum operating temperature of RAFM steels fabricated by melting process is limited up to about 873 K (600 °C). Application of oxide dispersion strengthening (ODS) to RAFM steels is one of the promising ways to improve performance as a structural material for fusion reactors, because the application increases the maximum operating temperature and improves the radiation resistance.

Based on this concept, creep strengths of PM2000,[3] MA957,[4] 12YWT,[5] and F4,[6] which are typical "ferritic" ODS steels with high Cr contents and "martensitic" ODS steels with lower Cr contents such as ODS Eurofer 97[7,8] and JAEA 9Cr-ODS steels,[9,10] have been studied. In general, the creep strength of martensitic ODS steels is lower than that of ferritic ODS steels. However, the martensitic ODS steels have isotropic properties: There is no big difference in creep strength between parallel and transverse directions to the rolling direction.[6,8–10] The hoop creep strength (1000 hours at 973 K (700 °C)) for ferritic (F4) and martensitic (M11) steel tubes, were ranging from 130 to 151 MPa, but we could not find a significant difference in creep strength in the transverse direction for ferritic/martensitic ODS steels.[6,9,10] In any case, the transverse direction creep strength of ODS steels is generally higher than that of the strongest ferritic/martensitic high Cr steel produced by melting practice.[11]

Modern ferritic/martensitic ODS steels for fusion reactors contain Ti of about 0.3 pct (mass percent, unless noted otherwise) besides Y_2O_3 of about 0.3 pct. Many researchers agree that Y_2O_3 powder, which is added as raw material, dissolves into the matrix during mechanical alloying (MA)[12,13] and nanoscaled complex oxide particles, for example, $Y_2Ti_2O_7$, Y_2TiO_5, or Y-, Ti-, and O-enriched nanoclusters of 1 to 5 nm, and then form with a very high number density during the consolidation and heat-treatment processes. This has been supported through transmission electron microscopy with energy dispersive spectroscopy (TEM-EDX),[3,5,10,14] three-dimensional atom probe analysis (3DAP),[15,16] and small angle neutron scattering (SANS).[17] The creep strength of ferritic ODS steel with no Ti was certainly much lower than that of ferritic ODS steel with Ti.[3] Therefore, the aforementioned nanoscaled oxide particles or clusters are certainly realized by adding Ti and cause an ultrahigh creep strength of ferritic/martensitic ODS steels.

M. TAMURA, formerly Professor, Materials Science and Engineering Department, National Defense Academy, Yokosuka 2398686, Japan. Contact e-mail: mtamura.1943@pep.ne.jp H. SAKASEGAWA and H. TANIGAWA, Researchers, Fusion Research and Development Directorate, and K. SHIBA, Researcher, Nuclear Science and Engineering Directorate, are with the Japan Atomic Energy Agency, Ibaraki 3191195, Japan. K. SHINOZUKA, Research Associate, and H. ESAKA, Professor, are with the Materials Science and Engineering Department, National Defense Academy.
Manuscript submitted: December 20, 2009.
Article published online March 8, 2011

It was believed that Y-Ti complex oxides formed in ODS steels such as $Y_2Ti_2O_7$ have better thermal stability than Y_2O_3, and the size of $Y_2Ti_2O_7$ was still ultrafine at high temperatures, which contribute to the superior creep strength for a long time.[6,18] However, Miller et al.[15] reported a result using 3DAP. They showed that particle sizes of Y-, Ti-, and O-enriched particles were unstable, contrary to expectations, and their size largely increased after annealing at 1573 K (1300 °C) for 24 hours. Alinger et al.[19] also reported that the number density and volume fraction of the nanoscaled clusters decreased and their size increased with increasing consolidation temperature. Yamashita et al.[20] showed that the chemical composition of complex Y-Ti oxide particles in martensitic ODS steels after normalizing and subsequent tempering was not stoichiometric, and the Y/Ti ratio of the complex oxides ranged from 1.3 to 2.1. Ukai et al.[9] confirmed that precipitates found in a normalized martensitic ODS steel, M11, were Y-Ti oxides of 3 nm, but they also reported that nanoscaled particles of Y_2O_3 were mainly observed in the normalized and tempered condition of M11.[9] In addition to this, Otsuka et al.[10] reported that the creep strength of a furnace-cooled martensitic ODS steel was stronger than that of normalized and tempered martensitic ODS steels. These observations suggest that the addition of Ti is essential for the ODS steels, but the Y-Ti complex oxides are not stable and can change their nature during thermal exposures.

Under these circumstances, Shiba and Nakamura applied an ODS technique to the RAFM steel, F-82H, and introduced a newly designed ODS steel, named J1.[21] Its transverse creep strength was comparable to the ferritic ODS steels of the highest strength levels.[22]

In this study, the effect of normalizing and tempering condition and aging on the precipitation behavior of J1 was studied in order to improve the creep performance of J1 and to clarify the precipitation behavior of complex Y-Ti oxides formed in martensitic ODS steels. Many studies on ODS steels were done using sophisticated equipment, TEM-EDX, 3DAP, and SANS. These studies clarified that very fine particles of 1 to 5 nm were almost uniformly dispersed in the matrix of ODS steel, which is believed to be the reason for the high creep strength. However, 3DAP analysis also showed that the Y, Ti, and O amounts calculated from the average size and number density of these very fine particles were relatively small, at most 10 pct for martensite matrix[3] and 20 pct for ferrite matrix[15] of the total Y, Ti, and O contents of the steels. The nature of the remainder for each element was still unclear. In this study, the behavior of the remainders for each element was particularly focused using X-ray diffraction (XRD) and inductively coupled plasma (ICP) spectroscopy for extracted residues.

II. EXPERIMENTAL PROCEDURE

Chemical composition of J1 is Fe-0.16 pct C-0.013 pct Si-0.18 pct V-0.01 pct Ni-7.85 pct Cr-1.9 pct W-0.19 pct Ti-0.29 pct Y-0.17 pct O-0.1 pct Ta-0.01 pct N. Contents of Mn, P, S, Co, Mo, and Nb were below each detectable

limit: 0.01, 0.005, 0.002, 0.01, 0.01, and 0.01 pct, respectively. Insoluble Al and soluble Al in aqua regia were 0.001 pct and below 0.001 pct, respectively. J1 was prepared by MA using premixed metal powders with Y_2O_3 powder in a high-energy attritor in an argon atmosphere. Mechanically alloyed flakes were then degassed and canned in mild steel. The canned MA powders were consolidated by hot isostatic pressing at 1423 K (1150 °C) and then finally hot rolled to 20-mm thickness. The hot-rolled plate was normalized at 1323 K (1050 °C) for 1 hour followed by tempering at 1023 K (750 °C) for 1 hour. All these processes were conducted by Kobelco Research Institute Inc. (Kobe, Japan).

The as-received J1 was renormalized at 1223 to 1523 K (950 to 1250 °C) for 1 hour followed by tempering at 1023 K (750 °C) for 2 hours. In order to investigate the effect of tempering time on the precipitation behavior, the renormalized J1 at 1323 K (1050 °C) was also tempered at 1023 K (750 °C) for 10,000 hours. As for the preparation of extracted residue, specimens were electrolyzed in a solution of 1 pct tetra-methyl ammonium chloride-10 pct acetyl acetone methanol electrolyte in volume (10 pct AA solution) using a reference potential of the saturated Calomel electrode plus 50 mV after removing the surface layer of heat-treated specimens. The residue was separated using a filter with 0.1-μm pores (Nuclepore Track-Etched Membrane filter by Whatman, Tokyo) placed on a filter base connected to a water aspirator. The average size of Y-Ti complex oxides observed by TEM and 3DAP was much smaller than the pore size of the filter. However, it was empirically possible to analyze the precipitation behavior of ultrafine oxides because of the clogging of the filter pores with extracted precipitates.

Extracted residues together with a filter were observed by XRD using a Cu K_α line, and integral breadth of a diffraction peak was converted to particle size using the Scherrer's relation.[23]

$$d = \frac{K\lambda}{\beta \cos \theta} \qquad [1]$$

where K, λ, β, and θ are the Scherrer's constant, the wavelength of X-ray, the integral breadth, and the Bragg angle, respectively. The term d is the apparent size of the crystalline particles perpendicular to the diffraction plane, and K was assumed to be unity for a cubic particle.[23] Broadening caused by the test equipment of XRD in observed integral breadths was corrected by using the standard Si powder made by the National Institute of Standards and Technologies (Boulder, CO).

The Y and Ti contents in the extracted residues were analyzed using ICP. Although extracted residues were mainly obtained by using a 10 pct AA solution, some residues were also obtained by using a solution of 6N HCl at 373 K (100 °C) in order to dissolve and exclude $M_{23}C_6$ from the residues, where M denotes metallic elements such as Cr, Fe, and W.

Standard $Y_2Ti_2O_7$ with the stoichiometric composition was synthesized as a reference. It was prepared at 1723 K (1450 °C) for 24 hours in air using high-purity Y_2O_3 and TiO_2 (anatase) powders.

III. RESULTS

A. Microstructure

Optical microstructure of the as-received J1 was tempered martensite with about 15 pct of δ-ferrite in area fraction, which was elongated along the rolling direction.[22] Its microstructure resembled the high chromium ODS martensitic steels reported by Ukai and co-workers.[9,10] The details of microstructures including TEM of J1 were presented in a previous article.[22] When normalizing temperature decreased to 1223 K (950 °C), the amount of δ-ferrite increased to about 20 pct or more. In contrast, when normalizing temperature increased from 1323 K to 1523 K (1050 °C to 1250 °C), the amount of δ-ferrite decreased to 10 pct.

B. Extracted Residue

1. Preliminary studies using filters with different pore sizes

The sizes of Y-Ti complex oxides or clusters formed in ODS steels were much smaller than the pore size usually used: 100 or 200 nm. Therefore, the appropriate pore size of filter was examined first. Measurement of the amount of extracted residue and chemical composition analysis using ICP was conducted using filters with different pores of 15, 50, 100, or 200 nm. The results are shown in Figure 1. The specimens renormalized at 1323 K (1050 °C) were used for these analyses, because the large amount of $M_{23}C_6$, which existed in the as-received (normalized and tempered) condition, could affect the ICP analysis of extracted residue. The amount of extracted residue increased with decreasing pore size. In Figure 1, the amounts of Y and Ti in the residues are plotted in the form of the ratio of recovered to total amount in steel, also called the yield rate, in percent. The amounts of Y and Ti in the residue for 200-nm pore filter were not measured, but they were considered to be the same as those for 100 nm, because the amount of extracted residue for 200 nm was the same as for 100 nm. The yield rate of Y and Ti in the extracted residues increased with the increasing amount of the extracted residues as clogging became more pronounced. Considerable amounts, more than 50 pct of total Y and Ti contents, were detected in the residues even when the pore size was as large as 100 nm.

Figure 2 shows the XRD analysis of the residues in Figure 1. Intensities of the reference compounds are drawn in arbitrary units in proportion to the intensities given in the powder diffraction file (PDF) by the International Center for Diffraction Data. The presence of $M_{23}C_6$, $Y_2Ti_2O_7$, and Ti_2O was confirmed referring to the PDF system, but the other compounds were not clearly identified. The integral breadth for the diffraction peak of $Y_2Ti_2O_7$ at 30.7 deg was about 0.9 deg for each filter examined. This value can be converted to a particle size of about 11 nm using the Scherrer's relation, Eq. [1].

The nanoscaled Y-Ti complex oxide particles of 1 to 5 nm reported in the literature cannot be correctly measured using XRD, because it was difficult to completely separate the foot of the peak corresponding to such small particles from the background. The peak would have to be several degrees wide. However, the size of the extracted particles, 11 nm, is smaller than the pore sizes, from 15 to 200 nm. Figure 2 shows that the filters with pores from 50 to 200 nm could extract ultrafine particles of $Y_2Ti_2O_7$ of about 11 nm. Therefore, although some ultrafine particles smaller than the pore size can pass through the filter, most ultrafine particles can stay on a flat portion of the filter or stay near the inlet or inside of pores due to clogging. The ICP data shown in Figure 1 indicated that the ratios of Y/Ti of the filters, 15-, 50-, and 100-nm pore size, were roughly the same. Therefore, Figures 1 and 2 indicate that the residues were composed of the same kinds of oxides, but had a different size distribution depending on the pore size. When a filter with 15-nm pores was used, the amounts of Y and Ti in the residue were comparable with the total amounts of each constituent element in J1. Therefore, it is firmly concluded that a filter with 15-nm pores is the best choice for this study. However, it took a very long time, about 2 weeks, to filter the electrolyzed solution for 1 g specimen. Consequently, it was reasonable to use the filter with 100-nm pores, although some ultrafine precipitated particles
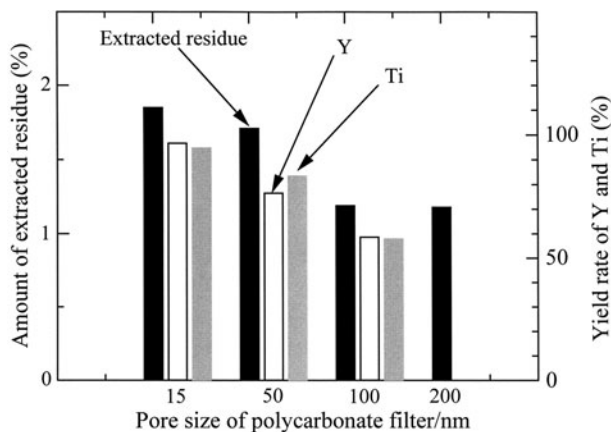

Fig. 1—Amount of extracted residue (left axis) for normalized J1 at 1323 K (1050 °C) using a filter having pores of 15, 50, 100, or 200 nm and yield rates of Y and Ti (right axis) in each residue.
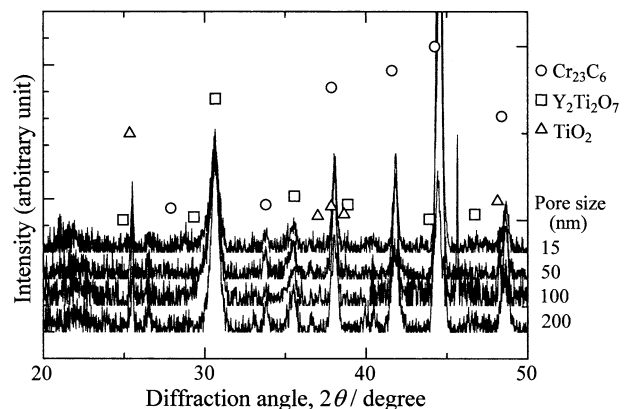

Fig. 2—XRD patterns corresponding to Fig. 1. Pore size is shown in the right axis.

should mix in the filtered solution. The filter with 100-nm pores was used for the subsequent studies.

2. *Precipitation in as-received J1*

The XRD pattern of the as-received J1 is shown in the bottom of Figure 3(a). Precipitation of $M_{23}C_6$, $Y_2Ti_2O_7$, and TiO_2 (anatase) was confirmed, and a very weak diffraction peak near 29 deg of Y_2O_3 was also observed. However, TiO_2 was not found for the as-received J1 in some cases.

A clear peak was observed at a diffraction angle of 24 deg beside these precipitates. This peak agreed with the strongest peak of Ti_2O_3 (described as $TiO_{1.51}$, in PDF No. 01-073-1781), although the subpeaks of Ti_2O_3 were not clear. Other compounds were not identified for this peak in the PDF system excepting WO_3. However, WO_3 is usually formed by hydrolyzing a solution that contains W ions. Its diffraction peaks are generally broad and WO_3 is not usually formed in an alcohol-based solution. Consequently, we identified a peak near 24 deg as Ti_2O_3. Okuda and Fujiwara[12] also identified this peak as Ti_2O_3.

In addition to these particles, TaC should precipitate because of the solubility limit at the normalizing temperature.[24] However, TaC was not confirmed. Although a diffraction peak was occasionally found near the strongest diffraction angle for Ta_2O_5, clear evidence for Ta compounds was not obtained by XRD. ICP analysis of the residue extracted from the as-received J1 showed that only 24 to 48 pct of total Ta content in J1 was detected in the residue for both as-received and renormalized specimens. This indicates that most Ta passed through the filter as nanoscaled particles or ions. Nanoscaled particles denote hereinafter the particles smaller than about 1 to 5 nm, which cannot be captured by the filter with 100-nm pores. An amorphous-like broad peak was frequently observed near 22 deg; however, this might not be a diffraction peak, but a ghost peak caused by a subtracting method of background intensity.
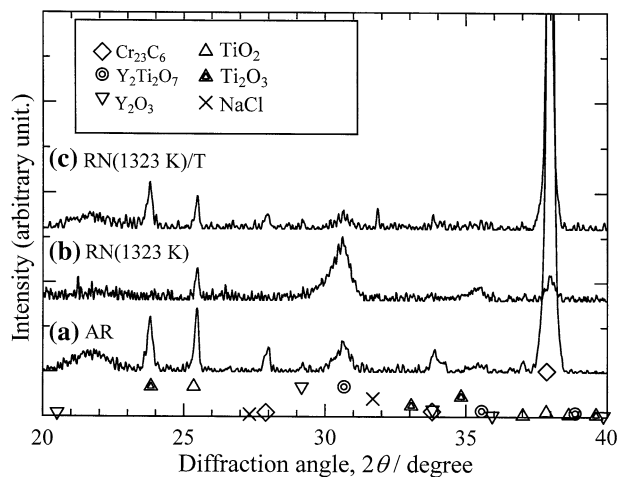

Fig. 3—XRD patterns of extracted residues of J1: (*a*) as-received, (*b*) renormalized at 1323 K (1050 °C) for 1 h, and (*c*) retempered at 1023 K (750 °C) for 2 h after renormalization.

Integral breadth of a diffraction peak can be converted to a particle size using Eq. [1]. The particle sizes of the as-received J1 shown in Figure 3(a) were as follows: 52 nm for (511) of $M_{23}C_6$, 15 nm for (222) of $Y_2Ti_2O_7$, 99 nm for (222) of Y_2O_3, 56 nm for (012) of Ti_2O_3, and 127 nm for (101) of TiO_2. Although these values were average values based on some assumptions for a tremendous number of particles extracted on a filter, the previous work[25–27] confirmed that the measured sizes by XRD for several kinds of precipitates ranging 10 to 300 nm roughly coincided with the TEM observations.

3. *Characteristic feature of XRD pattern resulting from heat treatment*

Figure 3 also shows (b) diffraction patterns of both renormalizing at 1323 K (1050 °C) for 1 hour and (c) renormalizing followed by retempering at 1023 K (750 °C) for 2 hours. It is found by comparing Figures 3(a) and (b) that in the renormalized state of J1 (b), the peaks of Ti_2O_3 and Y_2O_3 were apparently and completely diminished, while the peaks of $M_{23}C_6$ almost disappeared as predicted. In addition, the peak height of TiO_2 of the renormalized state seemed to be lowered, compared to the peak heights of $Y_2Ti_2O_7$ and TiO_2.

On the other hand, as shown in Figure 3(c), the diminished peaks of Ti_2O_3 and Y_2O_3 after renormalizing appeared again after tempering, although there are some NaCl peaks for the renormalized and tempered specimen (c), which was caused by an error. It should be noted as an astonishing result that these formation and decomposition reactions of Ti_2O_3 and Y_2O_3 can reversibly take place at relatively low temperatures of normalizing and tempering.

It is difficult to specify the reactions that caused the appearance and disappearance of Ti_2O_3 or decrease and increase of the amount of TiO_2, accompanied by normalizing or tempering, because Ti could form several kinds of oxides. However, although compounds containing Y were only $Y_2Ti_2O_7$ and Y_2O_3, the appearance and disappearance of Y_2O_3 by tempering and normalizing took place. This phenomenon indicates that tempering should cause decomposition of some $Y_2Ti_2O_7$ particles and formation of relatively large Y_2O_3 particles about 100 nm extracted by the filter with 100-nm pores, although most of the aforementioned oxide particles passed through the filter, as already discussed in Section I.

Figure 4 shows XRD patterns of (a) the as-received J1, (b) the further tempered J1 (1023 K (750 °C) for 1000 hours), and (c) the renormalized and tempered J1 (N: 1523 K (1250 °C) for 1 hour and T: 1023 K (750 °C) for 2 hours. The peak height of $M_{23}C_6$ at 38 deg for each specimen in Figure 4 was made the same in order to compare the relative intensities of other compounds. From the comparison of Figures 4(a) and (b), we found that the peak heights of $Y_2Ti_2O_7$ and TiO_2 decreased and those of Y_2O_3 and Ti_2O_3 contrarily increased with increasing time of tempering from 2 to 1000 hours. From the comparison of Figures 4(a) and (c), we found also that the peak heights of $Y_2Ti_2O_7$ and
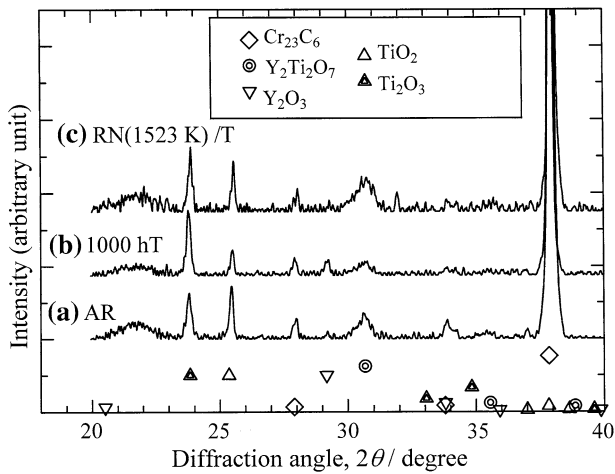
Fig. 4—XRD patterns of extracted residues of J1: (*a*) as-received, (*b*) further tempering at 1023 K (750 °C) for 1000 h, and (*c*) renormalized at 1523 K (1250 °C) for 1 h followed by tempering at 1023 K (750 °C) for 2 h.
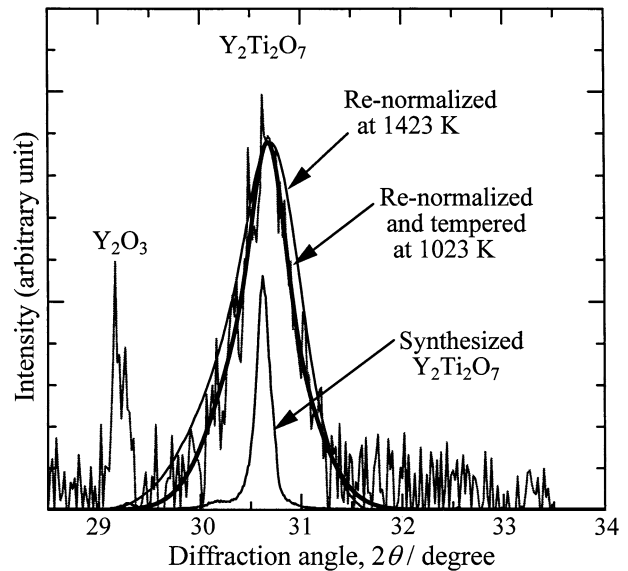

Fig. 5—Comparison of diffraction peaks of $Y_2Ti_2O_7$ from extracted residues from the renormalized J1 at 1423 K (1150 °C), the renormalized and subsequently retempered at 1023 K (750 °C), and the synthesized one.

Ti_2O_3 seemed to be larger (compare also Figure 4(c) to Figure 3(c)). Although it is well known that Y_2O_3, $Y_2Ti_2O_7$, TiO_2, and Ti_2O_3 are stable compounds, Figures 3 and 4 really indicate that these oxides ranging from 10 to 100 nm formed in J1 were not so stable and easily decomposed and formed, depending on normalizing and tempering conditions.

If the decomposition of $Y_2Ti_2O_7$ takes place during tempering, changes in the peak profiles of $Y_2Ti_2O_7$ should be expected. Figure 5 shows diffraction profiles of $Y_2Ti_2O_7$ in the extracted residue of J1 renormalized at 1423 K (1150 °C) comparing it with one that was artificially synthesized. The main peak of the synthesized $Y_2Ti_2O_7$ agreed with that of stoichiometric $Y_2Ti_2O_7$. Besides this main peak, weak peaks were observed at 29.3 and 30.2 deg for the synthesized $Y_2Ti_2O_7$. $Y_2Ti_2O_7$ has a cubic lattice and forms a pyrochlore type solid solution, P_{ss}. The phase diagram of the Y_2O_3-TiO_2 system[29] shows that the chemical composition of P_{ss} ranges from the stoichiometric composition to the Y_2O_3 enriched composition by about 3 mole pct at just below 1603 K (1330 °C) and the solid solution can largely dissolve Y_2O_3 at higher temperatures. Hexagonal Y_2TiO_5 is an equilibrated phase with P_{ss} at 1723 K (1450 °C),[29] the temperature at which $Y_2Ti_2O_7$ used in this study was synthesized in air, but any corresponding peaks to Y_2TiO_5 could not be found. Therefore, the subpeak at 29.3 deg is considered not to correspond to either equilibrated or precipitated Y_2O_3, but to unreacted Y_2O_3. The equilibrated phase with Y_2O_3 at 1723 K (1450 °C) is a fluorite type solid solution with a cubic lattice. The fluorite solid solution dissolves TiO_2 of about 40 to 50 mole pct, and the phase boundary between the fluorite solid solution and P_{ss} at high temperatures is not clear. Lattice constant of the solid solution linearly changes with increasing Y_2O_3 content from 67 mol pct Y_2O_3 in $Y_2Ti_2O_7$ to 60 mole pct Y_2O_3-40 mole pct TiO_2.[30] This change corresponds to the changes in diffraction angle of 29.8 to 30.7 deg, where

the center is 30.25 deg. Hence, a mixture of solid solution, which consists of fluorite and pyrochlore types, could make the subpeak of the synthesized $Y_2Ti_2O_7$ at 30.2 deg shown in Figure 5.

A peak profile of the normalized J1 shown in Figure 5 is asymmetric and has a tail at lower angle. Therefore, the extracted residue of the normalized J1 possibly contained a considerable amount of $Y_2Ti_2O_7$ enriched with Y_2O_3, P_{ss}, in addition to stoichiometric $Y_2Ti_2O_7$. It was reported that nanoscaled particles or clusters found in ODS steels had core/shell structures, the precipitate cores were Y rich, while the shell regions were enriched in Ti, Cr, or V.[31,32] Therefore, P_{ss}, the presence of which was estimated in the residue of the normalized J1, possibly contained these elements, Cr and V, although the lattice constant of a fluorite or pyrochlore type solid solution dissolving these elements is not yet available in the literature.

In the figure, the diffraction intensity of retempering at 1023 K (750 °C) after normalizing at 1423 K (1150 °C) is also plotted, and the diffraction pattern is serrated due to the coexistence of large particles of $M_{23}C_6$, which make up the majority in the residue. In this specimen, the peak at 29.2 deg is clearly observed and this is the main peak of Y_2O_3. The serrated peak excluding the part of Y_2O_3 was fitted by a bimodal normal distribution curve. A bold line represents a regression curve adjusting the diffraction angle and the peak height to the summit position of the renormalized one. The integral breadth of the renormalized specimen is large and the peak profile is largely tailing toward a low diffraction angle as compared to the subsequently retempered one. Therefore, we can say that the tempering of J1 caused the decomposition of the stoichiometric compound of $Y_2Ti_2O_7$ and P_{ss}, which dissolved more Y_2O_3 in $Y_2Ti_2O_7$.
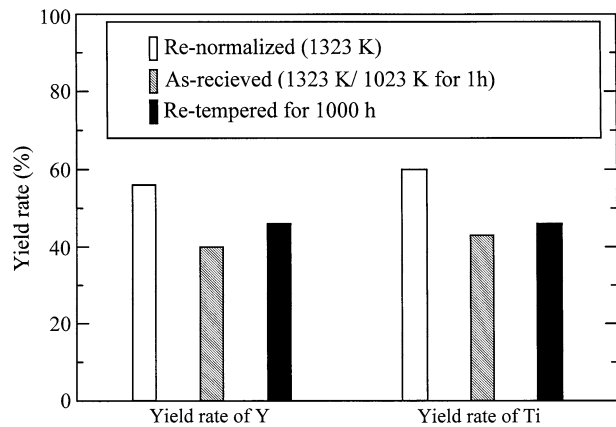
Fig. 6—Yield rates of Y and Ti in the extracted residues of J1. The as-received steel is conditioned to be normalized and tempered at 1023 K (750 °C) for 1 h condition. "Renormalized" denotes that as-received J1 is renormalized at 1323 K (1050 °C), and "retempered for 1000 h" denotes that the as-received J1 was tempered further for 1000 h at 1023 K (750 °C).

4. ICP analysis

In the preceding Sections III–B–2 and III–B–3, it was shown that fine oxide particles in J1 were possibly decomposed and reformed by heat treatment. Figure 6 shows the yield rates of Y and Ti in the extracted residues of the specimens renormalized at 1323 K (1050 °C) (white bars), normalized and tempered at 1023 K (750 °C) for 1 hour, as-received (hatched gray bars), and the as-received J1 tempered further at 1023 K (750 °C) for 1000 hours (black bars). The variations in the ICP data for both elements are similar. Regarding the as-renormalized state, about 60 pct of Y and Ti remained on a filter as Y- and Ti-containing compounds. On the other hand, in the as-received state, which represented the normalizing and tempering at 1023 K (750 °C) for 1 hour condition, only about 40 pct of the total Y or Ti was detected on a filter. Therefore, the difference of about 20 pct of Y or Ti containing particles or ions passed through a filter after tempering. This indicated that some of the Y and Ti containing particles must have decomposed to ions or subdivided into nanoscaled particles on tempering.

During further tempering for 1000 hours, the yield rates of Y and Ti tended to recover to the renormalized state, although the yield rates decreased once by 2 hours of tempering. That is, a reverse reaction seems to take place between short-time tempering and long-term tempering. However, as shown in Figures 3 and 4, the compounds precipitated during tempering were the same, i.e., $M_{23}C_6$, $Y_2Ti_2O_7$, TiO_2, Ti_2O_3, and Y_2O_3, for both tempering conditions: 2 and 1000 hours at 1023 K (750 °C). This could be explained if the growth of $Y_2Ti_2O_7$ or Y_2O_3 and Ti_2O_3 particles, which formed through the decomposition of $Y_2Ti_2O_7$, took place. This would cause the increase in the yield rates of Y and Ti.

5. Relation between precipitation and normalizing temperature

The compound of $Y_2Ti_2O_7$ is a stable phase described in the equilibrium phase diagram of the Y_2O_3-TiO_2
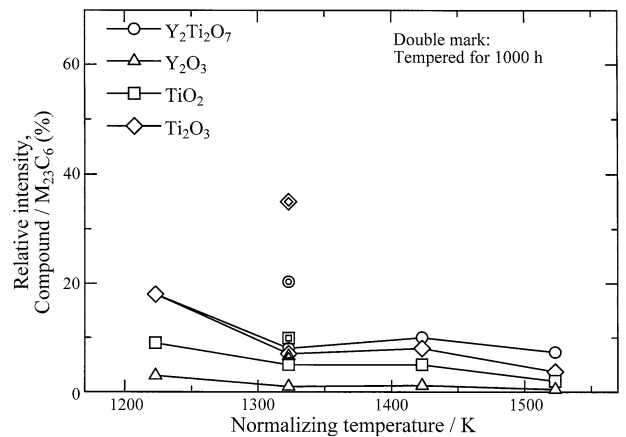

Fig. 7—Relative intensity of precipitated compounds, $Y_2Ti_2O_7$, Y_2O_3, TiO_2, and Ti_2O_3, formed by tempering at 1023 K (750 °C) for 2 h are presented as a function of normalizing temperature. Relative intensity after 1000 h tempering is also shown by double marks.

system.[29] However, Figures 3 through 6 indicated that some of the fine particles of $Y_2Ti_2O_7$ formed in J1 at the normalizing temperature possibly decomposed during subsequent tempering. In order to reconfirm this phenomenon, the precipitation behavior of J1 was analyzed as a function of normalizing temperature.

Precipitates in the renormalized J1 at 1223 to 1523 K (950 to 1250 °C) were confirmed to be $Y_2Ti_2O_7$, TiO_2, and $M_{23}C_6$. Neither Y_2O_3 nor Ti_2O_3 were found. After subsequent tempering at 1023 K (750 °C) for 2 hours, a great amount of $M_{23}C_6$ was found together with $Y_2Ti_2O_7$ and TiO_2. In addition, Y_2O_3 and Ti_2O_3 were also found. The amounts of these compounds were estimated by the following method.

It was confirmed by ICP analyses that the Cr content in the residues was nearly constant, 16.5 pct, after tempering at 1023 K (750 °C) for 2 hours, independent of the normalizing temperature. Since the Cr content in $M_{23}C_6$ formed in high Cr martensitic steels was roughly 60 pct,[26] the amount of $M_{23}C_6$ formed in the normalized and tempered J1 should be roughly constant. Therefore, the integrated intensities of $Y_2Ti_2O_7$, TiO_2, Ti_2O_3, and Y_2O_3 were divided by the integrated intensity of (420) $M_{23}C_6$. The calculated relative intensities for each compound are presented in Figure 7 as a function of normalizing temperature. Relative amounts for each compound were high, when the normalizing temperature was 1223 K (950 °C). On the contrary, they decreased when the normalizing temperature was 1323 K (1050 °C). The relative amounts for $Y_2Ti_2O_7$, TiO_2, Y_2O_3, and Ti_2O_3 decreased slightly or stayed the same with increasing normalizing temperature. However, the relative amounts for these compounds of the 1000 hours tempered specimen, as shown by the double marks in the figure, increased largely. This increase suggested that the coarsening of the compounds listed in Figure 7 progressed during long-term tempering and many particles were captured by the filter.

Figure 8 shows the changes in yield rates of Y and Ti under two conditions: normalized only and normalized and tempered, as a function of normalizing temperature.
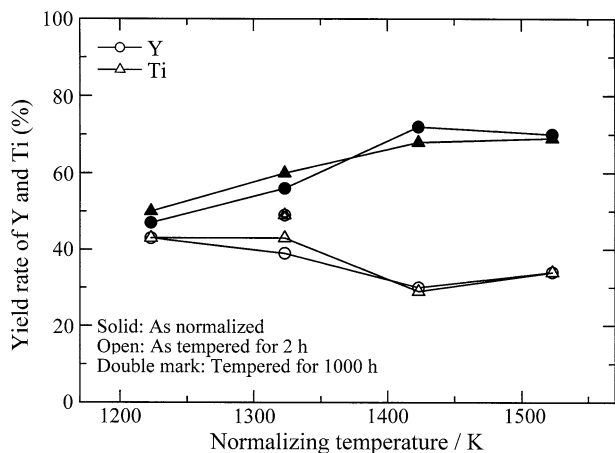
Fig. 8—Yield rates of Y and Ti of the extracted residues for the normalized, and the normalized and subsequently tempered, specimens are presented as a function of normalizing temperature. The yield rates for 1000 h tempering are also shown by double marks.

Fig. 9—XRD patterns of powders: (*a*) synthesized $Y_2Ti_2O_7$; (*b*) heating the synthesized $Y_2Ti_2O_7$ at 1023 K (750 °C) for 2 h; (*c*) heating the mixture of the synthesized $Y_2Ti_2O_7$ and extracting residue of $M_{23}C_6$ at 1273 K (1000 °C) for 2 h; and (*d*) heating the mixture of the synthesized $Y_2Ti_2O_7$, extracting residue of $M_{23}C_6$ and Ti at 1273 K (1000 °C) for 2 h.

The data of 1000 hours tempering at 1023 K (750 °C) are also presented in Figure 8. No compounds containing Y other than $Y_2Ti_2O_7$ were found in the extracted residues of the normalized only specimens. Moreover, the changes in the yield rate of Ti in the normalized only specimens were roughly the same as the yield rate of Y. Therefore, the yield rate of Y in the normalized specimen could be explained mainly by $Y_2Ti_2O_7$, although we found minor peaks for TiO_2. It is found that the yield rate for Y and Ti is about 70 pct in the normalized specimens at 1523 K (1250 °C) and 1423 K (1150 °C). On the contrary, at 1423 K (1150 °C) and lower temperatures, the yield rate for Y and Ti decreased with the decrease in normalizing temperature. Since as pointed out by Miller[15] the oxide particle size in austenite increases by heating at high temperatures, the yield rate of Y and Ti could increase with an increase in normalizing temperature on the reasonable assumptions that the total amount of $Y_2Ti_2O_7$ formed in austenite of J1 was roughly constant independent of normalizing temperature and the yield rate for Y and Ti was largely independent on the average size of particles.

After the subsequent tempering of the specimens normalized at 1423 K (1150 °C) and 1523 K (1250 °C), the yield rates of Y and Ti significantly decreased. In the tempered specimens, Y_2O_3 and Ti_2O_3 were additionally found. Consequently, one would expect the yield rates to increase due to these compounds, but the opposite was found. This could be expected if some $Y_2Ti_2O_7$ particles possibly decomposed during tempering and the decomposition products passed through the filter. The minimum amount of the decomposed $Y_2Ti_2O_7$ in the specimens normalized at 1423 K (1150 °C) and 1523 K (1250 °C) should be proportional to the difference in the yield rate of Y, *i.e.*, roughly 40 pct (= 70 to 30).

On the other hand, when normalized at 1223 K (950 °C), the yield rates of Y or Ti after subsequent tempering at 1023 K (750 °C) for 2 hours were about the same as the rates in the normalized specimen. This suggests that the decomposition of $Y_2Ti_2O_7$ hardly took place, when the normalizing temperature was
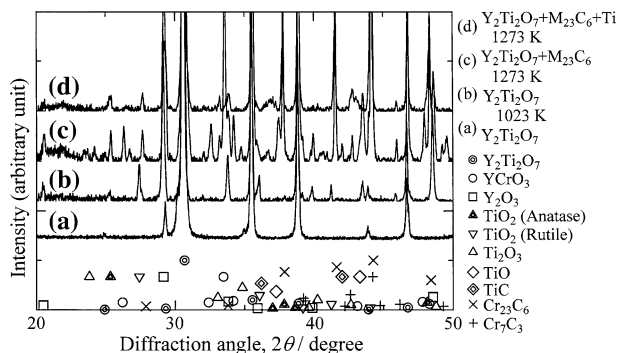
1223 K (950 °C). However, this explanation seems inadequate. It would be reasonable that the fraction of the decomposition of $Y_2Ti_2O_7$ is roughly the same regardless of the normalizing temperature, and the yield rates of Y and Ti in tempered specimens decrease with decreasing normalizing temperature. However, the observed yield rates for the tempered specimens, normalized at 1223 K (950 °C) and 1323 K (1050 °C) and tempered at 1023 K (750 °C) for 2 hours including 1000 hours tempering, were only slightly lower than for as-normalized specimens. Therefore, we propose that two opposing phenomena simultaneously occur to explain the observed results. When the normalizing temperature was low, the amount of δ-ferrite was large and the average particle size of $Y_2Ti_2O_7$ was small. These are also considered in Section IV.

The decomposition of the compound $Y_2Ti_2O_7$ raises many questions that need to be resolved. Nevertheless, the evidence that such a decomposition took place is implicit in Figures 3 through 8.

C. Chemical Property of $Y_2Ti_2O_7$

1. Stability of $Y_2Ti_2O_7$ synthesized in air

We start by showing the compatibility of the synthesized $Y_2Ti_2O_7$ with $M_{23}C_6$ and Ti, which could form in iron matrix. Figure 9 shows the XRD peaks for the samples: (a) the synthesized $Y_2Ti_2O_7$; (b) the synthesized $Y_2Ti_2O_7$ annealed at 1023 K (750 °C) for 2 hours in an open container made of SiO_2; (c) the mixture of synthesized $Y_2Ti_2O_7$ and $M_{23}C_6$ powders annealed at 1273 K (1000 °C) for 2 hours in a vacuum sealed capsule; and (d) a mixture of synthesized $Y_2Ti_2O_7$, $M_{23}C_6$, and Ti powder annealed at 1273 K (1000 °C) for 2 hours in a vacuum-sealed capsule. The powder of $M_{23}C_6$ was electrolyzed and extracted from an experimental steel composed of Fe-9 pct Cr-1 pct Mo. Most peaks of the synthesized $Y_2Ti_2O_7$ agreed with diffraction angles calculated referring to the PDF cards. Weak subpeaks near 30.2 and 35 deg, which were on the left shoulder of each peak of $Y_2Ti_2O_7$, and a weak subpeak at 29.3 deg were observed. These peaks corresponded to
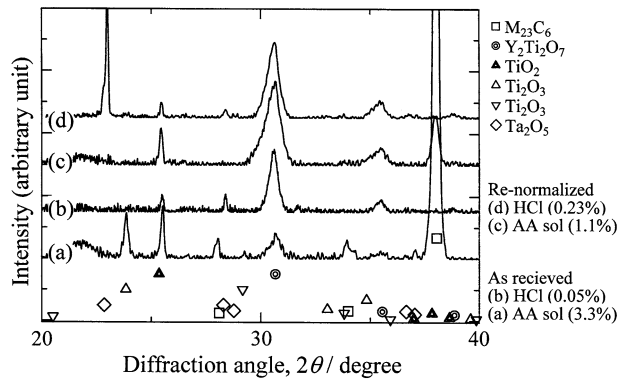
Fig. 10—XRD patterns of the extracted residues: (*a*) and (*b*) as-received J1 and (*c*) and (*d*) renormalized J1. (a) and (c) extracted residues using a 10 pct AA solution and (c) and (d) extracted residues using a 6 N HCl solution. The number in parentheses denotes the amount of extracted residue for each.

Table I. Durability in a 6 N HCl Solution for Precipitates in J1 and the Synthesized Compounds

Material	Durability in 6 N HCl
Standard	
Y_2O_3	completely soluble at room temperature
TiO_2 (anatase)	insoluble at 373 K (100 °C)
$Y_2Ti_2O_7$ (synthesized in air)	almost insoluble at 373 K (100 °C)
Precipitates in J1	
$M_{23}C_6$	almost soluble at 373 K (100 °C)
TiO_2 (anatase)	possibly soluble
Ti_2O_3	completely soluble
Y_2O_3	completely soluble
$Y_2Ti_2O_7$	possibly soluble

P_{ss} and unreacted Y_2O_3, respectively, as already explained using Figure 5. This indicated that the synthesized $Y_2Ti_2O_7$ was a stoichiometric compound with a very small amount of impurity. In Figure 9(b), we can see clear peaks for the stable phases of Y_2O_3, TiO_2 (both rutile and anatase), and TiO with peaks of $Y_2Ti_2O_7$. These clear peaks show that some synthesized $Y_2Ti_2O_7$ definitely decomposed to its constituents and other stable oxides when annealed at 1023 K (750 °C) in air. This temperature is much lower than the synthesis temperature of 1723 K (1450 °C).

When the synthesized $Y_2Ti_2O_7$ is annealed at 1273 K (1000 °C) with $M_{23}C_6$ in vacuum, as shown in Figure 9(c), there are Y_2O_3, $YCrO_3$, TiO_2 (both rutile and anatase), TiO, Ti_2O_3, and Cr_7C_3 other than the raw materials of $Y_2Ti_2O_7$ and $M_{23}C_6$. When Ti is added, in case (d), $M_{23}C_6$ is completely consumed and TiC is found. However, TiO and Cr_7C_3 are not observed. These results show that, even though Ti does not coexist, $M_{23}C_6$ carbide can promote the decomposition of $Y_2Ti_2O_7$ and form Ti_2O_3 with the formation of Y_2O_3, which is more stable in air than TiO_2. From Figure 9, it is concluded that the stoichiometric compound $Y_2Ti_2O_7$ formed in air is easily decomposed in the presence of $M_{23}C_6$ or Ti.

These results suggest that $Y_2Ti_2O_7$ in J1, which is stable at the normalizing temperatures, could decompose and form Y_2O_3, TiO_2, and Ti_2O_3 by $M_{23}C_6$ or soluble Ti in the matrix of J1 on tempering at 1023 K (750 °C).

2. Stability of $Y_2Ti_2O_7$ in a 6 N HCl solution
Figure 10 shows diffraction peaks of the extracted residues using different solutions for the as-received and renormalized J1. The solutions are a 10 pct AA solution and a 6 N HCl solution. Figure 10(a) shows the diffraction pattern for the extracted residue from the as-received J1 using a 10 pct AA solution. When the as-received J1 is directly dissolved in a 6 N HCl solution (Figure 10(b)), weak peaks of $Y_2Ti_2O_7$ at 35.6 and 39.0 deg can be detected easily, because the background becomes low due to the dissolution of $M_{23}C_6$ by HCl. However, peaks for both Y_2O_3 at 29.3 deg and

Ti_2O_3 at 23.9 deg were lost at the same time. Concerning the renormalized specimens (Figures 10(c) and (d)), both $Y_2Ti_2O_7$ and TiO_2 were observed and a strong peak for Ta_2O_5 was occasionally observed ((d)), although a small peak at 28.4 for (b) and (d) was not identified. It is very hard to see the durability of $Y_2Ti_2O_7$ in HCl by the simple comparison of the peak heights of the residues extracted using a 6 N HCl and a 10 pct AA solution. The amounts of the extracted residues were also shown in Figure 10. When considering the result using a 10 pct AA solution ((a) and (c)), the difference in the amounts of extracted residue between the as-received and renormalized specimens (3.3 – 1.1 = 2.1 pct) roughly corresponds to the amount of $M_{23}C_6$. This amount is in general agreement for similar heat-resistant steels. However, the value of about 1 pct of the residue extracted from the normalized J1 is much greater than the sum of Y, Ti, and O mass fractions, about 0.65 pct. Therefore, other elements such as Cr and V[31,32] than Y, Ti, and O are possibly contained in $Y_2Ti_2O_7$ formed in J1. The enrichment of Cr, V, and Ti is reported by Marquis[30] and Klimenkov *et al.*[31] as shell structures of the nanoscaled $Y_2Ti_2O_7$ type oxides precipitated in the martensitic/ferritic ODS steels.

On the other hand, when considering the results using a 6 N HCl solution, the amounts of the extracted residues were much lower than 1 pct. Consequently, not only Y_2O_3 and Ti_2O_3, but also $Y_2Ti_2O_7$, dissolved in the solution, because $Y_2Ti_2O_7$ was the major oxide in the extracted residue in the normalized J1. If $Y_2Ti_2O_7$ formed in J1 dissolves in an HCl solution, it can be concluded that TiO_2 in J1 also dissolves in an HCl solution from the comparison of the peak heights of $Y_2Ti_2O_7$ and TiO_2, as shown in Figures 10(a) and (b).

Table I shows the summary of Figure 10 with the results of beaker tests. It can be seen that $Y_2Ti_2O_7$ and TiO_2 (anatase) formed in J1 are soluble in HCl solution at 373 K (100 °C), although the synthesized ones in air were almost insoluble. This implies that the chemical properties of these compounds formed in the matrix of J1, $Y_2Ti_2O_7$, TiO_2, and Ti_2O_3, are different from those synthesized in air.

From the preceding discussion, $Y_2Ti_2O_7$ formed in J1 decomposed easier than the $Y_2Ti_2O_7$ synthesized in air.

The synthesized $Y_2Ti_2O_7$ also decomposed when placed in contact with $M_{23}C_6$ and Ti. These characteristics of $Y_2Ti_2O_7$ support the decomposition of $Y_2Ti_2O_7$ in J1 by the application of a heat treatment.
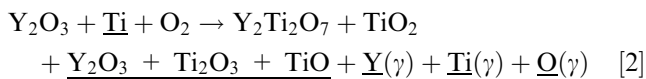
IV. DISCUSSION

A. *Modeling for decomposition of $Y_2Ti_2O_7$*

The experimental results clearly indicated that some $Y_2Ti_2O_7$ formed in J1 reversibly decomposed and reformed during the normalizing and tempering heat treatments. This conclusion was obtained from the XRD results of the extracted residues recovered from a 100-nm pore filter. However, we know that ODS steels are certainly strengthened by the dispersion of nano-scaled oxide particles, which should have passed through from the filter pores. Therefore, speculation regarding the behavior on the nanoscaled particles' possible reactions, which occur in J1 during the heat treatments, is discussed.

First, we consider the consolidation process of ODS steel. Previous work[12] described that when Y_2O_3 powders were mechanically alloyed with metal powders in the presence of Ti in a high-energy attritor, Y_2O_3 decomposed to soluble Y and O atoms in the steel matrix in a metastable condition and at the same time oxygen gas, which adhered to metal powders and ball mill elements, and was impurity in an argon atmosphere, was dissolved in the metal matrix. During subsequent hot isostatic pressing and normalizing, the nanoscaled complex oxide particles of $Y_2Ti_2O_7$ formed by combining with the solute Ti.
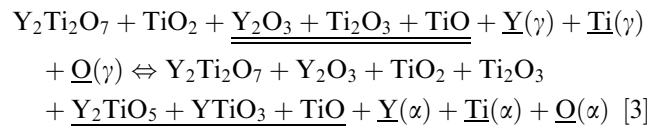
The reactions during the consolidation processes and the normalizing can be summarized qualitatively by the following equation:

$$Y_2O_3 + \underline{\underline{Ti}} + O_2 \rightarrow Y_2Ti_2O_7 + TiO_2$$
$$+ \underline{\underline{Y_2O_3 + Ti_2O_3 + TiO}} + \underline{Y}(\gamma) + \underline{Ti}(\gamma) + \underline{O}(\gamma) \quad [2]$$

where the underbar and double underbar denote solute atoms in the matrix and substances that pass perfectly through a filter and are not detected in the extracted residues, respectively. The left-hand side of Eq. [2] indicates a state before mechanical alloying, and O_2 denotes the excess and inevitable oxygen gas in an attritor ball mill. The excess oxygen concentration was 0.092 mass pct, the value obtained by subtracting oxygen concentration in Y_2O_3 from total oxygen concentration in the steel. The right-hand side corresponds to a state after normalization. Solute atoms of Y, Ti, and O should exist thermodynamically in the normalized J1, because we confirmed $Y_2Ti_2O_7$ and TiO_2 in J1. Nano-scaled particles of $Y_2Ti_2O_7$, which pass through a filter, should exist in J1, as confirmed in the similar ODS steels,[16,20,22,32] but the double underbar was omitted for simplicity. If both Ti and TiO_2 coexist, Ti_2O_3 and TiO thermodynamically exist also, because the oxygen potentials of these oxides are between Ti and TiO_2. Y_2O_3 could exist for the same reason. However, these were not confirmed on the filter residues. Therefore, all

of these compounds are indicated by the double underbar, although the amounts of these are unknown. In Eq. [2], a description for P_{ss} was omitted, because the chemical composition of P_{ss} is close to the stoichiometric $Y_2Ti_2O_7$. Although P_{ss} precipitated in J1 possibly contained Cr and V, as discussed in Section III–C–2, a description for this was omitted for simplicity. We confirmed Ta_2O_5 occasionally in the extracted residues, and therefore, more stable oxide SiO_2 should exist. However, these are omitted in Eq. [2], because the amounts formed were considered to be small.

From Figure 3, it was found that some of the $Y_2Ti_2O_7$ particles that existed in the normalized J1 were replaced by Ti_2O_3 and Y_2O_3 during subsequent tempering. After tempering for 1000 hours at 1023 K (750 °C), at least four kinds of oxides, $Y_2Ti_2O_7$, TiO_2, Y_2O_3, and Ti_2O_3, were observed, although neither Y_2O_3 nor Ti_2O_3 existed in the residues before tempering. However, Y_2O_3 and Ti_2O_3 disappeared from the residues and $Y_2Ti_2O_7$ was found again when the steels were renormalized. That is, the decomposition and reformation reactions of $Y_2Ti_2O_7$ were reversible on normalizing and tempering. Hence, the following equation can be written for a qualitative description:

$$Y_2Ti_2O_7 + TiO_2 + \underline{\underline{Y_2O_3 + Ti_2O_3 + TiO}} + \underline{Y}(\gamma) + \underline{Ti}(\gamma)$$
$$+ \underline{O}(\gamma) \Leftrightarrow Y_2Ti_2O_7 + Y_2O_3 + TiO_2 + Ti_2O_3$$
$$+ \underline{\underline{Y_2TiO_5 + YTiO_3 + TiO}} + \underline{Y}(\alpha) + \underline{Ti}(\alpha) + \underline{O}(\alpha) \quad [3]$$

The left- and right-hand side of Eq. [3] correspond to normalized and tempered conditions, respectively. The notations in Eq. [3] are the same as in Eq. [2]. Figure 11 shows the locations of these compounds in the Y_2O_3-TiO_2-Ti ternary diagram. In the diagram, possible regions of stability for J1 at the normalizing and tempering temperatures are shown schematically. The experimental results obtained by XRD indicate that the normalized J1 was in equilibrium with the region that included $Y_2Ti_2O_7$, P_{ss}, and TiO_2 and the tempered J1
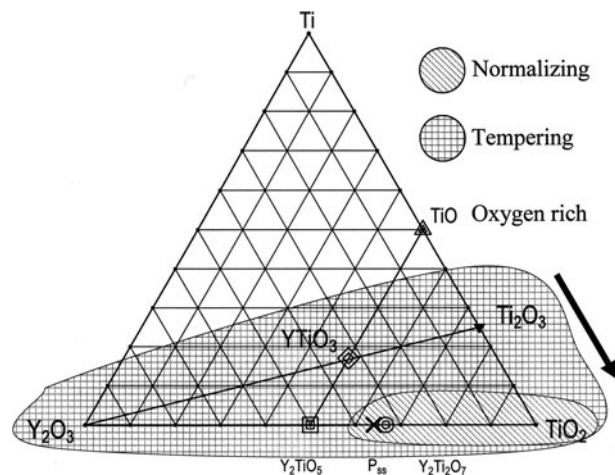

Fig. 11—Y_2O_3-TiO_2-Ti phase diagram (mole fractions). Regions in equilibrium with J1 in the normalized, and the normalized and subsequently tempered, states are shown schematically.
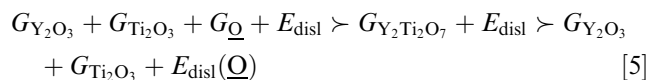
with the region including Y_2O_3, Ti_2O_3, TiO_2, and $Y_2Ti_2O_7$. The compound of $YTiO_3$ was not confirmed by XRD for the tempered J1. Since Ti_2O_3 and Y_2O_3 were confirmed in the residue, more stable compounds of $YTiO_3$ than Y_2O_3 and Ti_2O_3 may exist, depending on the condition of the heat treatment.

Although it is impossible to discuss in detail the substances that are not in the residue, Eq. [3] can be simplified as follows:

$$Y_2Ti_2O_7(\gamma) \Leftrightarrow Y_2O_3 + Ti_2O_3 + \underline{O}(\alpha) \quad [4]$$
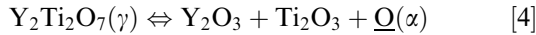
where $\underline{O}(\alpha)$ denotes soluble oxygen in the matrix. Decomposition of $Y_2Ti_2O_7$ implies that Y and Ti atoms diffused out from the compound, and the formation of Y_2O_3 and TiO_2 implies that nucleation and growth processes should occur, and hence, many nanoscaled particles besides large particles of Y_2O_3 and TiO_2 should form. Therefore, a considerable amount of the nanoscaled Y and Ti particles must have passed through the filters, and so, the yield rates of Y and Ti for the tempered states were lower than those of the normalized states, as shown in Figures 6 and 8. However, Eq. [4] predicts clearly that tempering temporarily increases soluble oxygen in the ferritic matrix. Reliable data on the solubility limit of oxygen in alpha and gamma iron are limited, but the solubility limit of oxygen in alpha iron is considered to be lower than that of gamma iron.[33] Moreover, phase stability calculations including metastable stages show $Y_2Ti_2O_7$ to be more stable than Y_2O_3 and TiO_2.[28,29,34] Therefore, if Eq. [4] is true, additional explanation is necessary.

Many dislocations exist before tempering, and $M_{23}C_6$ is formed during tempering. $M_{23}C_6$ could assist the decomposition of $Y_2Ti_2O_7$, as shown in Figure 9, and forms $YCrO_3$, Cr_7C_3, and so on. However, these Cr compounds were not confirmed in our experiments. Therefore, $M_{23}C_6$ is not directly responsible for the decomposition of $Y_2Ti_2O_7$. On the other hand, dislocations introduced by normalizing have a very strong interaction with the solute oxygen atoms. This was evidenced by the 3DAP observations by Miller.[16] Therefore, dislocations induced before tempering can absorb the excess soluble oxygen presented by Eq. [4] during tempering. In other words, although it is usually not feasible that the reaction of Eq. [4] progress from the left to right hand, if the interaction energy between dislocations and the soluble oxygen atoms is large, decomposition of $Y_2Ti_2O_7$ is possible. This means that the following equation should stand up for the decomposition of $Y_2Ti_2O_7$:

$$G_{Y_2O_3} + G_{Ti_2O_3} + G_{\underline{O}} + E_{disl} \succ G_{Y_2Ti_2O_7} + E_{disl} \succ G_{Y_2O_3}$$
$$+ G_{Ti_2O_3} + E_{disl}(\underline{O}) \quad [5]$$

where $G_{Y_2O_3}$ and so on are formation free energies of each substance, E_{disl} is the internal energy due to induced dislocations, and E_{disl} (O) is the internal energy of dislocations to which solute oxygen atoms are segregated. That is, the interaction energy between dislocations and solute oxygen atoms, defined by the term $E_{disl}(O) - E_{disl} - G_{\underline{O}}$, is negative, or the relation of

$E_{disl} + G_{\underline{O}} \succ E_{disl}(O)$ is required. This is supported by the 3DAP observations by Miller.[16] In addition, the bonding force of $Y_2Ti_2O_7$ particles formed in J1 was found to be not as strong as that of the synthesized $Y_2Ti_2O_7$.

It has been already reported that the introduction of dislocations decomposes stable compounds, such as carbides. Wilson[35] showed that when quenched martensite is plastically deformed and then tempered, precipitation of ε-carbide was inhibited and the well-known first stage of tempering was bypassed. This was interpreted as the clustered carbon about dislocations being more stable than ε-carbide.[36] Kubota et al.[37] showed that even the stable carbide of NbC, which precipitated in austenite, dissolved by cold working and subsequent tempering. Tamura et al.[25,38] recently showed that NaCl carbonitrides precipitated in a martensitic steel dissolved during tempering with the help of dislocations. In this way, redistribution of solute atoms around dislocations causing the decomposition of stable compounds was established in many experimental results. Therefore, the reversible reaction presented in Eq. [4] can be rewritten as follows:

$$Y_2Ti_2O_7\{in\ \gamma\} \Leftrightarrow Y_2O_3 + Ti_2O_3 + disl(\underline{O})\{in\ \alpha\} \quad [6]$$
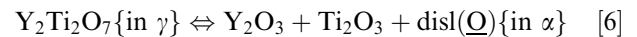
where $disl(\underline{O})$ denotes soluble oxygen trapped by dislocations. Figure 12 shows a schematic drawing of Eq. [6]. When normalizing, dislocations are annealed out and the free oxygen proceeds to form $Y_2Ti_2O_7$ in gamma iron.

B. Variation in yield rate of Y and Ti

Assuming that Eq. [6] is true and some of the nanoscaled particles formed by this reaction passed through a filter, the decrease in the yield rates of Y and Ti due to tempering, as shown in Figures 6 and 8, could be qualitatively explained. The increased yield rates of the normalized state with increasing normalizing temperature could be explained also assuming the growth of oxide particles during normalization at high temperatures. However, the fact that the yield rates after tempering increased with lowering of the normalization temperature was not yet explained satisfactorily. However, neither induced dislocations by normalization nor $M_{23}C_6$ formed during tempering can simply explain the variation of the yield rates shown in Figure 8, because the dislocation density or the amount or distribution of $M_{23}C_6$ does not depend much on the normalizing temperature. On the other hand, the amount of δ-ferrite indeed increases with decreasing normalizing temperature.

Figure 13 shows SEM microstructures of the longitudinal cross section of as-received J1. Finely dispersed white contrast was mainly due to $M_{23}C_6$ and the precipitation free zone, deformed in the rolling direction, was observed as about 15 pct in area fraction and we called this δ-ferrite. δ-ferrite was surrounded by coarse $M_{23}C_6$ particles. The EDX results are shown in Table II. Positions 1 and 2 are the matrix of δ-ferrite and tempered martensite, respectively. Chemical compositions
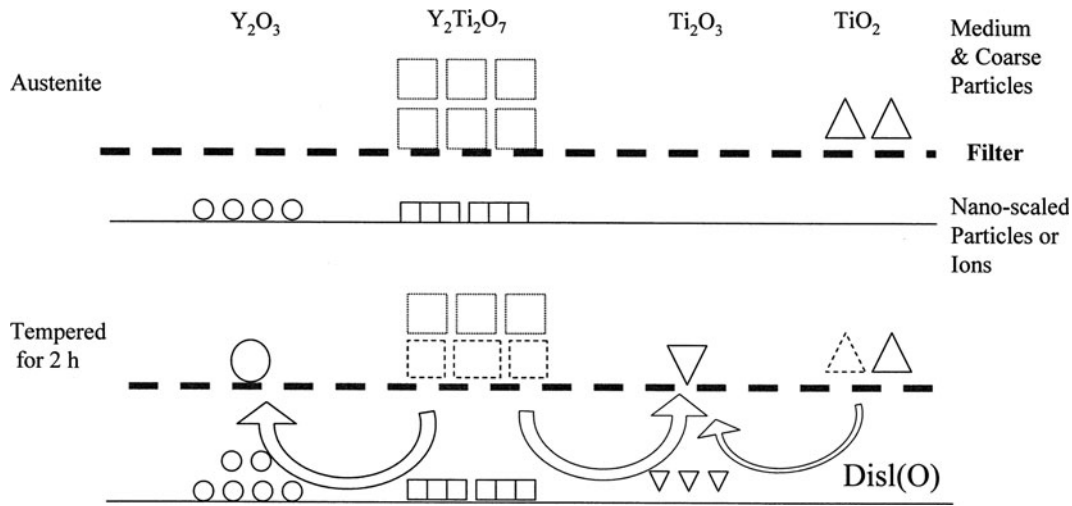
Fig. 12—Decomposition of $Y_2Ti_2O_7$ and TiO_2 by tempering is illustrated schematically. Large symbols denote precipitates on a filter and small ones denote nanoscaled particles or ions, which passed through a filter. Dotted symbols denote dissolved compounds by tempering. Disl(O) denotes soluble excess oxygen atoms trapped by dislocations.
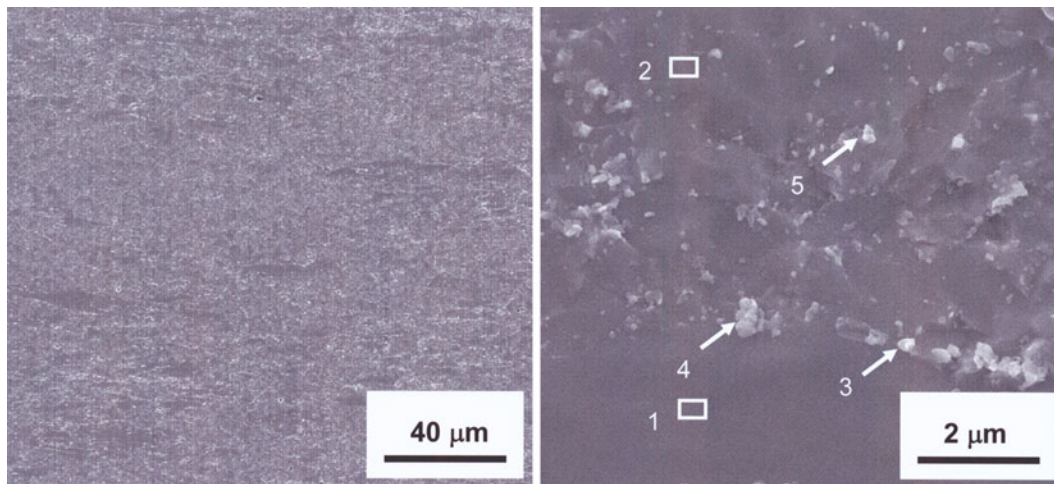

Fig. 13—SEM images of longitudinal cross section of as-received J1. EDX analyses of the positions shown by numbers are given in Table II.

Table II. Chemical Compositions for Marked Positions Indicated in Fig. 13 (Mass Percent)

Position	Cr	Fe	W	V	Ti	Y	Remarks
1	7.7	86.5	2.44	0.29	0.14	<0.1	δ-ferrite
2	7.5	86.2	2.11	<0.1	0.23	0.33	martensite
3	17.9	68.5	5.54	0.41	0.25	0.49	$M_{23}C_6$
4	15.3	75.4	3.42	<0.1	0.18	0.49	$M_{23}C_6$
5	15.4	76.6	2.18	<0.1	<0.1	<0.1	$M_{23}C_6$

analyzed resembled to the chemical composition of J1, although Y in δ-ferrite and V in martensite were not detected at a significant level. Although the matrix might affect the EDX results for positions 3 through 5, these particles were considered to be $M_{23}C_6$, because their Cr content was higher than the matrix. These results suggested that $M_{23}C_6$ precipitated on a boundary between martensite and δ-ferrite included Y-, V-,

or Ti-oxide particles, because the thermodynamic calculations[39] indicate that $M_{23}C_6$ dissolves little V and Ti, although the data regarding Y are not available. Ukai et al.[9] also reported that $M_{23}C_6$ found in a 9 pct Cr martensitic ODS steel contained Ti.

Table III shows coherency with $M_{23}C_6$ or Fe matrix of typical Y-, Ti-, Cr-, Fe-, V-, and Ta-oxides referring to the phase diagrams. Coherency was defined as a ratio of a lattice constant of a compound to the lattice constant of $M_{23}C_6$ or iron. The averaged values shown using an asterisk were calculated for Y_2O_3, $Y_2Ti_2O_7$, and Y_3TaO_7 against bcc iron based on "the cube on cube relation," i.e., the Baker–Nutting relation.[40] When the crystal system is not cubic, the most coherent value was listed and so only partial coherency is expected for these oxides. Many kinds of oxides have high coherency with both $M_{23}C_6$ and the matrix, and most of them have higher coherency with $M_{23}C_6$ than the bcc matrix. Especially $Y_2Ti_2O_7$, Y_2O_3, and Y_3TaO_7

Table III. Coherency with $M_{23}C_6$ and Fe of Typical Oxides Possibly Formed in J1; When a Compound is not Cubic, the Most Coherent Value is Calculated and, Therefore, Only Partial Coherency is Expected for these Compounds

Substance	Crystal System	Lattice Constant (A)			Coherency			Remarks
		a	b	c	$M_{23}C_6$	Bcc Fe	Fcc Fe	
Y_2O_3	cubic	10.60	—	—	0.99	1.02*	0.98	—
$Y_2Ti_2O_7$	cubic	10.09	—	—	0.95	0.97*	0.93	Y_2O_3-$2TiO_2$
Y_2TiO_5	orthorhombic	10.35	3.70	11.25	0.97	0.90	—	Y_2O_3-TiO_2
$YTiO_3$	orthorhombic	5.68	7.60	5.34	1.00	0.99	—	Y_2O_3-Ti_2O_3
$YCrO_3$	orthorhombic	5.52	7.53	5.24	0.98	0.97	—	Y_2O_3-Cr_2O_3
$YFeO_3$	orthorhombic	5.28	5.59	7.60	0.99	0.92	—	Y_2O_3-Fe_2O_3
$Y_{10}V_2O_{20}$	monoclinic	10.06	7.85	13.96	0.94	0.88	—	$5Y_2O_3$-V_2O_5
Y_3TaO_7	cubic	10.52	—	—	0.99	1.02*	0.97	$3Y_2O_3$-Ta_2O_5
TiO	cubic	4.18	—	—	1.18	1.10	—	—
Ti_2O_3	rhombohedral	5.15	—	13.63	0.97	0.90	—	—
TiO_2 (anatase)	tetragonal	3.79	—	9.51	0.89	0.83	—	—
$Cr_{23}C_6$	cubic	10.66	—	—	<u>1.00</u>	0.93	0.99	—
Bcc Fe	cubic	2.86	—	—	1.07	<u>1.00</u>	—	—
Fcc Fe	cubic	3.60	—	—	—	—	<u>1.00</u>	—

Asterisked values denote the average of coherency based on the Baker–Nutting relation.

are cubic, and these compounds are elastically more stable in $M_{23}C_6$ than the matrix. Moreover, the compound Ti_2O_3 produced by the decomposition of $Y_2Ti_2O_7$ may be also stable in $M_{23}C_6$, although it is rhombohedral. This shows a possibility that $M_{23}C_6$ forms colonies of compounds with $Y_2Ti_2O_7$, Y_2O_3, and Ti_2O_3. Due to the predictable high diffusion rate near the boundaries between δ-ferrite and martensite matrix, precipitates grow rapidly, so that the mixed colonies of $M_{23}C_6$, $Y_2Ti_2O_7$, and Y_2O_3 in the form of $M_{23}C_6$ can be formed. Therefore, the yield rates of Y and Ti, as shown in Figure 8, increased with decreasing normalizing temperature, *i.e.*, increase in the amount of δ-ferrite. When normalizing, most of the $M_{23}C_6$ particles dissolve in gamma iron and relatively large particles of $Y_2Ti_2O_7$ are reformed from Y- and Ti-compounds, which increase in the yield rates of Y and Ti.

When the smaller $Y_2Ti_2O_7$ particles decompose on tempering, Y, Ti, and O diffuse in a state of atom and coarsen the larger $Y_2Ti_2O_7$ particles. Therefore, long-time tempering of 1000 hours could increase the yield rate for Y and Ti, as shown in Figures 6 and 8. In addition to this reason, existence of $M_{23}C_6$ should be taken into account. As shown in Table III, $YCrO_3$ and $YFeO_3$ are complex oxides having high coherency with $M_{23}C_6$ as compared with the matrix, although the coherency is partial. Therefore, thermodynamic data for these complex oxides are not available yet, but when, in addition to $Y_2Ti_2O_7$ and Ti_2O_3, these compounds form in $M_{23}C_6$, total elastic energy could decrease. Figure 9 shows that $YCrO_3$ forms by heating $M_{23}C_6$ and $Y_2Ti_2O_7$ at 1273 K (1000 °C), although this heating temperature is much higher than the service or tempering temperatures of ODS steels. If these situations could happen and the colonies of $M_{23}C_6$ and nanoscaled oxide particles form, redistribution of the nanoscaled oxide particles should progress, which causes the increase in the yield rates of Y and Ti after 1000 hours tempering, as shown in Figures 6 and 8.

C. *Future study*

In this study, it was clarified based on the experiments that fine $Y_2Ti_2O_7$ particles of about 10 nm decomposed to Y_2O_3 and Ti_2O_3 during tempering. This brings to mind the degradation of creep strength after long-term service. However, the redistribution of these oxides could occur through the pipe diffusion of oxygen accompanying the formation of a large number of nanoscaled oxides or clusters along dislocations. Therefore, even though the redistribution of the precipitates may happen, so long as the considerable amount of dislocations exists, the speed of the degradation of creep strength may not be so large, because the nanoscaled particles are continuously formed. In other words, when dislocations are exhausted after long-time service, the redistribution rate of $Y_2Ti_2O_7$ also slows, leading to a plateau in degradation.

However, on inverse transformation, retained dislocations supply not only many precipitation sites for nanoscaled particles but also diffusion paths to coarsen the pre-existing particles such as $Y_2Ti_2O_7$, which could lead to a decrease in the number of nanoscaled particles that are formed during normalization and tempering. Therefore, for martensitic ODS steels, in order to keep high creep resistance, it is important to optimize the fabrication processes, *i.e.*, working and heating processes.

Usually, the strengthening constituent of TaC with 10 nm is found in the extracted residues of the Ta-containing high Cr martensitic steel; however, in the residues of J1, only 24 to 48 pct of total Ta was detected and the Ta-containing compounds were seldom found except as Ta_2O_5. However, one of the reasons for high creep strength of J1 is that this steel contains Ta. Y_3TaO_7 is a stable compound, so that Y_2O_3 and Ta_2O_5 could form Y_3TaO_7 in J1 and Y_3TaO_7 itself has high coherency with the matrix of alpha and gamma iron, as shown in Table III. Therefore, Ta could form nanoscaled Y_3TaO_7 particles and increase creep resistance. However, since Y_3TaO_7 was not detected by XRD and

has the same crystal system and similar lattice constant with $Y_2Ti_2O_7$, Y_3TaO_7 may form a solid solution with the nanoscaled $Y_2Ti_2O_7$. Y_3TaO_7 has high coherency with $M_{23}C_6$ as well, so Ta could be contained in $M_{23}C_6$ as coprecipitated oxides. Lu et al.[41] recently reported that Ta-rich carbides were not observed in Eurofer 97, the chemical composition of which was similar to J1, and Ta was found in a relatively large Y_2O_3 particle. In any case, Ta certainly increases the creep strength of J1 and may be Eurofer 97; therefore, the situation of Ta should be clarified in the near future.

The model proposed for the precipitation sequence, schematically shown in Figure 12, is based on several speculations. Therefore, further studies using TEM, 3DAP, and other sophisticated techniques are necessary for evaluating the model. Measuring oxygen solubility in alpha and gamma phases of the matrix of J1 is also an essential issue.

V. CONCLUSIONS

Extracted residues of an oxide-dispersion-strengthened high chromium martensitic steel, J1, were analyzed by X-ray and inductively coupled plasma atomic emission spectroscopy, and the following conclusions were obtained.

1. Fine particles of $Y_2Ti_2O_7$ with a small amount of coarse TiO_2 (anatase) particles formed by normalization.
2. By tempering at 1023 K (750 °C) for 2 h, Y_2O_3 and Ti_2O_3 formed and some $Y_2Ti_2O_7$ particles decomposed.
3. The Y_2O_3 and Ti_2O_3 disappeared and $Y_2Ti_2O_7$ reformed on renormalization. That is, the decomposition and reformation of $Y_2Ti_2O_7$ particles occurred reversibly.
4. Chemical properties of $Y_2Ti_2O_7$ formed in the ODS steel, J1, were different from the stoichiometric $Y_2Ti_2O_7$ synthesized in air. $Y_2Ti_2O_7$ in J1 dissolved other constituents, especially Y_2O_3's in its structure, which made it less stable.
5. The segregation of oxygen to dislocations introduced by normalization can also aid the decomposition and reformation of $Y_2Ti_2O_7$.
6. The carbide $M_{23}C_6$ formed during tempering has the same crystal structure and a very close lattice constant to Y_2O_3, which suggests that $M_{23}C_6$ could provide a favorable site for Y_2O_3, and thus help with the decomposition of $Y_2Ti_2O_7$ on tempering.

REFERENCES

1. K. Shiba, M. Enoeda, and S. Jitsukawa: *J. Nucl. Mater*, 2004, vols. 329–333, pp. 243–47.
2. M. Tamura, H. Hayakawa, M. Tanimura, A. Hishinuma, and T. Kondo: *J. Nucl. Mater.*, 1986, vols. 141–143, pp. 1067–73.
3. R.L. Klueh, J.P. Shingledecker, R.W. Swindeman, and D.T. Hoelzer: *J. Nucl. Mater.*, 2005, vol. 341, pp. 103–14.
4. A. Alamo, V. Lambard, Z. Averty, and M.H. Mathon: *J. Nucl. Mater.*, 2004, vols. 329–333, pp. 333–37.
5. R.L. Klueh, P.J. Maziasz, I.S. Kim, L. Heatherly, D.T. Hoelzer, N. Hashimoto, E.A. Kenik, and K. Miyahara: *J. Nucl. Mater.*, 2002, vols. 307–311, pp. 773–77.
6. S. Ukai, T. Okuda, M. Fujiwara, T. Kobayashi, S. Mizuta, and H. Kawashima: *J. Nucl. Sci. Technol.*, 2002, vol. 39, pp. 872–79.
7. R. Lindau, A. Möslang, M. Schirra, P. Schlossmacher, and M. Klimenkov: *J. Nucl. Mater*, 2002, vols. 307–311, pp. 769–72.
8. A. Möslang, E. Diegele, M. Klimiankov, R. Lässer, R. Lindau, E. Materna-Morris, C. Petersen, R. Pippan, J.W. Rensman, M. Rieth, B. van der Schaaf, H.-C. Scheider, and F. Tavassoli: http://www-pub.iaea.org/mtcd/meetings/PDFplus/fusion-20-preprints/FT_p. 1–21.
9. S. Ukai, T. Kaito, S. Ohtsuka, T. Narita, M. Fujiwara, and T. Kobayashi: *ISIJ Int.*, 2003, vol. 43, pp. 2038–45.
10. S. Ohtsuka, S. Ukai, and M. Fujiwara: *J. Nucl. Mater.*, 2006, vol. 351, pp. 241–46.
11. M. Taneike, F. Abe, and K. Sawada: *Nature*, 2003, vol. 424, pp. 294–96.
12. T. Okuda and M. Fujiwara: *J. Mater. Sci. Lett.*, 1995, vol. 14, pp. 1600–03.
13. Y. Kimura, S. Takaki, S. Suejima, R. Uemori, and H. Tamehiro: *ISIJ Int.*, 1999, vol. 39, pp. 176–82.
14. S. Ukai and M. Fujiwara: *J. Nucl. Mater.*, 2002, vols. 307–311, pp. 749–57.
15. M.K. Miller, D.T. Hoelzer, E.A. Kenik, and K.F. Russell: *J. Nucl. Mater.*, 2004, vols. 329–333, pp. 338–41.
16. M.K. Miller, E.A. Kenik, K.F. Russell, L. Heatherly, D.T. Hoeler, and P.J. Maziasz: *Mater. Sci. Eng.*, 2003, vol. 353, pp. 140–45.
17. M.J. Alinger, G.R. Odette, and D.T. Hoelzer: *J. Nucl. Mater.*, 2004, vols. 329–333, pp. 382–86.
18. S. Ukai and S. Ohtsuka: *Mater. Jpn.*, 2005, vol. 44, pp. 749–56.
19. M. Alinger, G. Odette, and D. Hoelzer: *Acta Mater.*, 2009, vol. 57, pp. 392–406.
20. S. Yamashita, N. Akasaka, and S. Ohnuki: *J. Nucl. Mater.*, 2004, vols. 329–333, pp. 377–81.
21. K. Shiba: private communication, 2003.
22. K. Shinozuka, M. Tamura, H. Esaka, K. Shiba, and K. Nakamura: *J. Nucl. Mater.*, 2009, vol. 384, pp. 1–5.
23. F.W. Jones: *Proc. R. Soc. A*, 166, vol. 166, pp. 16–43.
24. M. Tamura, H. Kusuyama, K. Shinozuka, and H. Esaka: *J. Nucl. Mater.*, 2007, vols. 367–370, pp. 137–41.
25. M. Tamura, M. Nakamura, K. Shinozuka, and H. Esaka: *Metall. Mater. Trans. A.*, 2008, vol. 39A, pp. 1060–76.
26. M. Tamura, H. Kusuyama, K. Shinozuka, and H. Esaka: *ISIJ Int.*, 2007, vol. 47, pp. 317–26.
27. M. Tamura, Y. Haruguchi, M. Yamashita, Y. Nagaoka, K. Ohinata, K. Ohnishi, E. Itoh, H. Ito, K. Shinozuka, and H. Esaka: *ISIJ Int.*, 2006, vol. 46, pp. 1693–1702.
28. R.S. Roth, J.R. Dennis, and H.F. McMurdie, eds.: *Phase Equilibrium Diagrams*, The American Ceramic Society, Westerville, OH, 1887, vol. 6, pp. 181–82.
29. N. Mizutani, A. Kitazawa, and M. Kato: *Nippon Kagaku Kaishi*, 1974, No. 9, pp. 1623–28.
30. E.A. Marquis: *Appl. Phys. Lett.*, 2008, vol. 95, 181904, pp. 1–3.
31. M. Klimenkov, R. Lindau, and A. Möslang: *J. Nucl. Mater.*, 2009, vols. 386–388, pp. 553–56.
32. S. Ohtsuka, S. Ukai, M, Fujiwara, T. Kaito, and T. Narita: *J. Nucl. Mater.*, 2004, vols. 329–333, pp. 372–76.
33. J.H. Swisher and E.T. Turkdogan: *Trans. TMS-AIME*, 1967, vol. 239, pp. 426–31.
34. A.E. MacHale and R.S. Roth, eds.: *Phase Equilibrium Diagrams*, The American Ceramic Society, Westerville, OH, 1896, vol. 12, p. 112.
35. D.V. Wilson: *Acta Metall.*, 1957, vol. 5, pp. 293–302.
36. M. Cohen: *Trans. JIM*, 1968, vol. 9, Suppl., pp. XXIII–XXIX.
37. H. Kubota, I. Kozasu, H. Kido, and T. Shimizu: *Tetsu-to-Hagané*, 1968, vol. 54, pp. 954–66.
38. M. Tamura: *Ferrum*, 2009, vol. 14, pp. 347–52.
39. B.G. Sundman, B. Jansson, and J.-O. Andersson: *CALPHAD*, 1985, vol. 9, pp. 153–90.
40. R.G. Baker and J. Nutting: *ISI Spec. Rep.*, ISI Pub., London, 1959, No. 64, pp. 1–22.
41. Z. Lu, R.G. Faulkner, N. Riddle, F.D. Martino, and K. Yang: *J. Nucl. Mater.*, 2009, vols. 386–388, pp. 445–48.